ACS Catalysis

LETTER

pubs.acs.org/acscatalysis

Synthesis of Homogeneous Pt-Bimetallic Nanoparticles as Highly Efficient Electrocatalysts

Chao Wang,[†] Miaofang Chi,[‡] Dongguo Li,[†,§] Dennis van der Vliet,[†] Guofeng Wang,[∥] Qiyin Lin,[†] John F. Mitchell,[†] Karren L. More,[‡] Nenad M. Markovic,[†] and Vojislav R. Stamenkovic*[,†]

[†]Materials Science Division, Argonne National Laboratory, Argonne, Illinois 60439, United States

[‡]Division of Material Science and Technology, Oak Ridge National Laboratory, Oak Ridge, Tennessee 37831, United States

[§]Department of Chemistry, Brown University, Providence, Rhode Island 02912, United States

[∥]Department of Mechanical Engineering and Materials Science, University of Pittsburgh, Pennsylvania, Pennsylvania 15260, United States

ABSTRACT: Alloying has shown enormous potential for tailoring the atomic and electronic structures, and improving the performance of catalytic materials. Systematic studies of alloy catalysts are, however, often compromised by inhomogeneous distribution of alloying components. Here we introduce a general approach for the synthesis of monodispersed and highly homogeneous Pt-bimetallic alloy nanocatalysts. Pt_3M (where M = Fe, Ni, or Co) nanoparticles were prepared by an organic solvothermal method and then supported on high surface area carbon. These catalysts attained a homogeneous distribution of elements, as demonstrated by atomic-scale elemental analysis using scanning transmission electron microscopy. They also exhibited high catalytic activities for the oxygen reduction reaction (ORR), with improvement factors of 2−3 versus conventional Pt/carbon catalysts. The measured ORR catalytic activities for Pt_3M nanocatalysts validated the volcano curve established on extended surfaces, with Pt_3Co being the most active alloy.

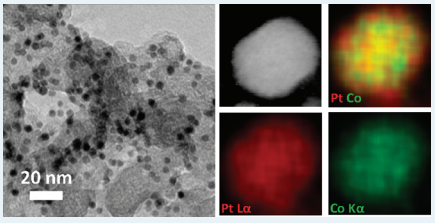

KEYWORDS: homogeneous alloy nanoparticles, Pt-bimetallic catalysts, oxygen reduction reaction, fuel cells, scanning electron microscopy

Alloy nanoparticles (NPs) have attracted increasing interest in the development of heterogeneous catalysts.[1−7] In an alloy catalyst, the employed elements may enhance the catalytic activity through ensemble[8] and/or electronic (ligand) effects.[9] With the broad choice of elements[3,5] and tuning of surface and near-surface compositions,[10,11] alloying provides numerous opportunities for the design of advanced catalysts with enhanced activity,[12,13] selectivity,[11,14,15] and durability.[16,17]

Although the average composition (based on bulk composition) is generally used to correlate with the catalytic behavior of an alloy catalyst, the distribution of elements within the NPs is found to have remarkable effects on the local electronic structures and catalytic behavior of the material.[4,18] Moreover, catalyst durability is highly dependent on the elemental homogeneity of an alloy catalyst. For example, one element may be more volatile than the other components in an alloy catalyst under specific reaction conditions, and a catalyst with an inhomogeneous distribution of the alloying components is thus less stable because of dissolution of the volatile element from the near-surface region.[19] The homogeneity of alloys and their compositional profiles have been successfully addressed on extended surfaces;[5,12,20] however, such insight to corresponding nanoscale alloy materials is still lacking. The treatments that are established to induce the proper elemental distribution on extended surfaces may not be always applicable to nanocatalysts for a number of reasons, such as particle sintering and the change of particle size that compromises the assessment of catalytic performance.[21,22] Therefore, a synthetic approach toward homogeneous alloy nanocatalysts is needed to achieve systematic advancement and fine-tuning of the catalytic properties in nanoscale systems.

Here we introduce the synthesis of monodisperse and highly homogeneous Pt-bimetallic alloy nanocatalysts. Previous research on extended surfaces of polycrystalline Pt_3M (M = Fe, Co, Ni, etc.) solid solution alloys has shown they are more active for the electrochemical reduction of molecular oxygen compared to pure Pt. The enhanced catalytic activity was found to vary with the altered d-band center position of these alloys, which led to reduced adsorption of oxygenated spectator species (e.g., OH^-).[5,12,20] On the other hand, Pt-bimetallic nanocatalysts prepared by conventional impregnation methods[19,21,23,24] usually possess compositional variance among the particles, that is, Pt-rich/-poor regions may even coexist in single NP,[19] which makes substantial difference in homogeneity of these materials compared to the bulk counterparts. Accordingly, the level of electronic modification by alloying element may not be uniform within the same catalyst, and hence, the catalytic performance is compromised. To achieve even distribution of elements, we use an organic solution approach to synthesize homogeneous Pt_3M alloy NPs by coupling the reduction of platinum acetylacetonate with the reduction of 3d transition metal salts or thermal decomposition of metal carbonyl. The obtained NPs are

Received: June 21, 2011
Revised: August 18, 2011
Published: August 25, 2011

supported on carbon black and then applied as electrocatalysts for the ORR. The dependence of the ORR activity on the alloying elements in the NPs is compared with the previous results obtained on extended surfaces,[5] with the aim of confirming the quality, and thereby homogeneity, of the alloy nanocatalysts by validating the consistency between these bimetallic systems.

EXPERIMENTAL METHODS

Nanoparticle Synthesis. Pt_3Fe NPs were synthesized by the simultaneous decomposition of $Fe(CO)_5$ and reduction of $Pt(acac)_2$. A 0.1 g portion of $Pt(acac)_2$ was dissolved in 10 mL of benzyl ether in the presence of 1 g of 1,2- tetradecanediol, 1 mL of oleylamine, and 1 mL of oleic acid. A 0.03 mL portion of $Fe(CO)_5$ was injected into this solution at 120 °C, and the solution temperature was then raised to 300 °C. The solution was cooled down after 30 min. Thirty milliliters of ethanol was added to precipitate the NPs, and the product was centrifuged (6,000 rpm). The obtained NPs were then dispersed in hexane. Pt_3Co NPs were synthesized by decomposition of $Co_2(CO)_8$ and reduction of $Pt(acac)_2$ in diphenyl ether following the previously reported recipe.[25]

Pt_3Ni NPs were synthesized by coreduction of $Pt(acac)_2$ and $Ni(ac)_2$.[26,27] $Ni(ac)_2$ (0.2 mmol) was dissolved in 10 mL of diphenyl ether in the presence of 0.5 mL of oleic acid, 0.5 mL of oleylamine, and 2 mmol of tetradecanediol. $Pt(acac)_2$ (0.33 mmol) dissolved in 1 mL of 1,2-dichlorobenzene was injected into this solution at 200 °C. The solution was kept at this temperature for 1 h and then cooled down to room temperature. The product was separated by adding 30 mL of ethanol and centrifuged (6,000 rpm).

Materials Characterization. Transmission electron microscopy (TEM) images were collected using a Philips EM 30 (200 kV). The compositions of the alloy catalysts were measured by energy-dispersive X-ray spectroscopy (EDS) for a large assembly of catalyst particles (a few hundred NPs) via TEM. X-ray diffraction (XRD) patterns were collected on a PANalytical X'pert PRO diffractometer using Cu Kα radiation at room temperature. High-angle annular dark field (HAADF) scanning transmission electron microscopy (STEM) and EDS characterization of individual NPs, including spectrum imaging to produce elemental maps were conducted using a JEOL 2200FS TEM/STEM equipped with a CEOS aberration (probe) corrector and a Bruker-AXS X-Flash 5030 silicon drift X-ray detector. The microscope was operated at 200 kV, and the electron beam size was ~0.7 Å for imaging and ~2 Å for EDS analysis (probe current ~400−500 pA).

Electrochemical Studies. Electrocatalytic activities were measured by using a three-electrode electrochemical cell and a rotating disk electrode (RDE) with a potentiostat (Autolab 302). A saturated Ag/AgCl electrode and a Pt wire were used as reference and counter electrodes, respectively, in 0.1 M $HClO_4$ electrolyte. Electrochemical surface area (ECSA) of the catalyst was determined from the under potentially deposited hydrogen (H_{upd}) region by integration of the cyclic voltammetry (CV) and was used for normalization of the kinetic current density, that is, specific activity. All CVs were recorded after 100 potential cycles and were stable during electrochemical characterization. The catalyst loading on the glassy carbon electrode was adjusted to be 12 $\mu g_{Pt}/cm^2_{disk}$. All the potentials in this report were referenced against the reversible hydrogen electrode (RHE) and the readout currents were corrected for the ohmic *iR* drop.[28,29]

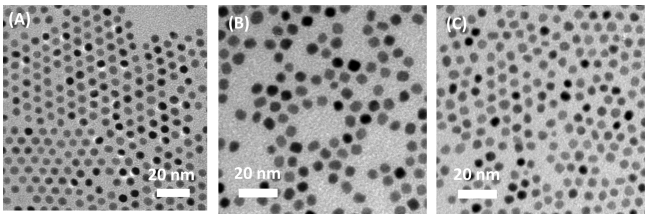

Figure 1. TEM images of the as-synthesized 5 nm (A) Pt_3Fe, (B) Pt_3Co, and (C) Pt_3Ni NPs.

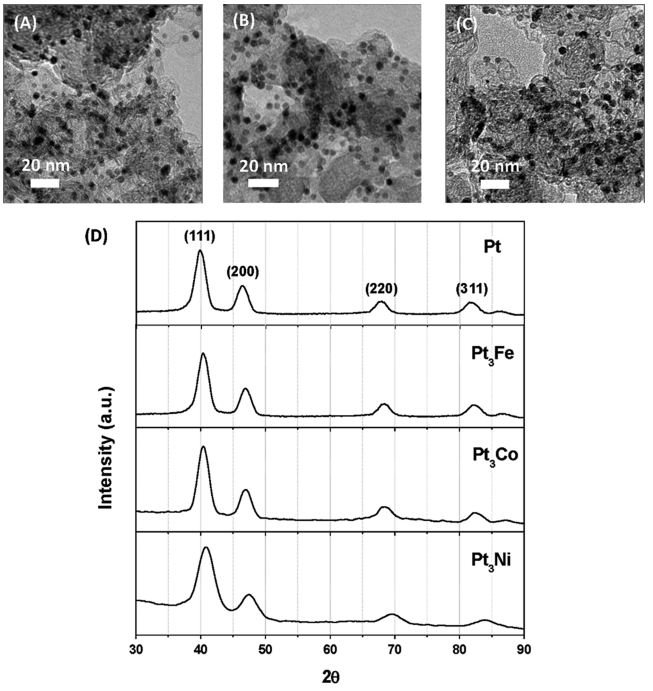

Figure 2. TEM images of the (A) Pt_3Fe/C, (B) Pt_3Co/C, and (C) Pt_3Ni/C catalysts after surfactant removal. (D) XRD patterns of the commercial 6 nm Pt/carbon catalyst and bimetallic Pt_3M/carbon catalysts prepared via organic solution synthesis in this work.

RESULTS AND DISCUSSION

NPs from organic solution synthesis possess the advantages of narrow size distribution and uniform shape.[30−32] This is beneficial for catalytic studies as the effects of particle size[33] and shape[34] can be differentiated from the others, for example, alloying. Figure 1 shows typical TEM images of the monodisperse ~5 nm Pt_3M NPs obtained from the organic solution synthesis. Our previous work has shown that the particle size can be tuned from <3 nm to ~10 nm,[33] and the alloy composition can be controlled to be from Pt-rich to 3d transition metal-rich by altering the synthesis procedures.[35] The focus of the present study is placed on the alloy homogeneity and elemental distribution within the NPs.

Since the as-synthesized particles were stabilized by organic surfactants in solution, they cannot be directly applied as a catalyst. To perform electrochemical characterization, these NPs were first supported on a high-surface-area carbon black (Tanaka, ~900 m^2/g), and then the surfactants were removed by heating in an oxygen rich atmosphere at ~180−200 °C. After this step, the obtained catalysts became electrochemically active,

dx.doi.org/10.1021/cs200328z |ACS Catal. 2011, 1, 1355–1359

and they were further annealed in a reducing atmosphere at 400 °C to reach the best catalytic performance without inducing significant particle sintering.[22] TEM images (Figure 2A−C) confirmed that no significant size or morphology change occurred after the thermal treatments. The prepared bimetallic catalysts exhibited an astonishingly homogeneous distribution of elements, as confirmed by the EDS elemental analysis acquired via HAADF-STEM. Figure 3 shows the elemental maps for Pt and Co acquired from a single nanoparticle. Both Pt and Co are homogeneously distributed within the NP and exhibit random element intermixing, as shown in the Pt−Co overlay map (Figure 3B), which provides direct evidence for highly homogeneous alloy catalyst.

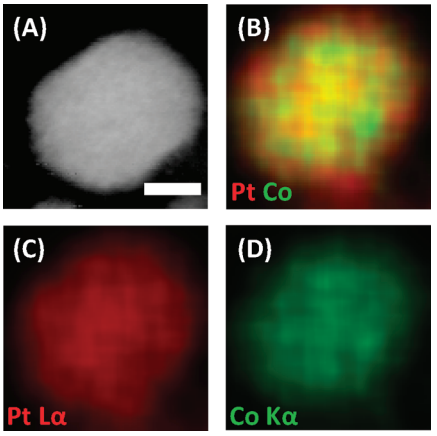

Figure 3. (A) HAADF-STEM image of the Pt_3Co/carbon catalyst and corresponding EDS elemental maps: (B) overlay of Pt and Co EDS maps, (C) Co−Kα, and (D) Pt-Lα. The scale bar in (A) is equal to 2 nm, which is also applicable for (B)−(D).

Additional proof that the NPs possess a uniform alloy composition was provided by XRD studies of the Pt_3M/carbon catalysts. The XRD patterns (Figure 2D) show that these bimetallic catalysts have the same face-centered cubic (fcc) structure as Pt, but with the diffraction peaks slightly shifted toward higher angles. This indicates random distribution of the 3d transition metal (Fe, Co and Ni) atoms in the Pt lattice and reduced Pt−Pt bond lengths in the formed solid solutions.[36,37] This observation together with the absence of peaks for other crystal phases (because of residual or excess metal phases)[21] demonstrates the uniform distribution of alloy elements within the NPs, that is, no significant composition variance among the catalyst NPs.

The obtained highly homogeneous alloy NP catalysts have led into a systematic investigation of the electrocatalytic performance of such Pt-bimetallic systems. Model catalyst studies for Pt_3M alloys on extended surfaces have established a volcano-type dependence of the ORR catalytic activity on the 3d transition metal (following the order in the element table, namely, Ti, V, Fe, Co, and Ni)[5] with Pt_3Co as the most active alloy.[12] To confirm this trend at the nanoscale, the ORR catalysis of the Pt_3M catalysts were studied by RDE measurements. Figure 4 summarizes the electrochemical characterization of the Pt_3M NPs. The voltammograms show H_{upd} peaks at E < 0.4 V and Pt oxidation/reduction peaks at 0.8−0.9 V in the anodic/cathodic scans, respectively. It is noteworthy that control of the particle size at ∼5−6 nm leads to consistent values for the specific surface area (between 30 and 40 m^2/g (Figure 4D)), which excludes the particle size effect in this study. Compared with Pt/carbon (6 nm Pt, from Tanaka), the Pt oxidation/reduction peaks of

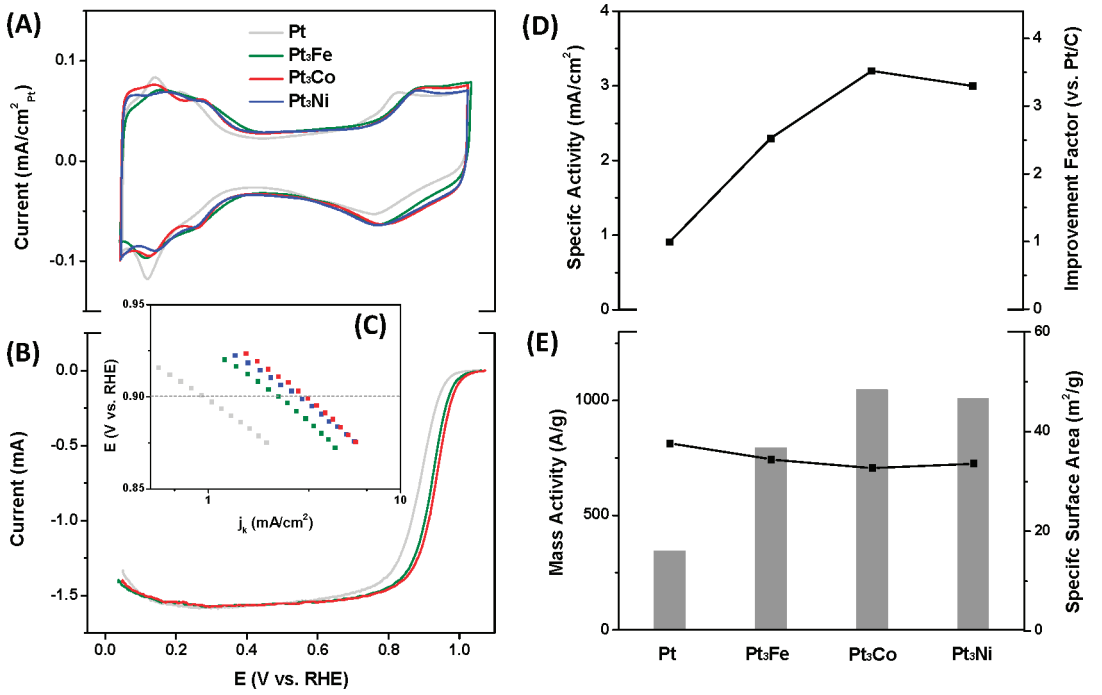

Figure 4. Electrocatalytic results of the Pt_3M/carbon catalysts for the ORR. (A) CVs recorded at 50 mV/s in Ar saturated 0.1 M $HClO_4$ at 60 °C. (B) Polarization curves recorded at 20 mV/s in O_2 saturated 0.1 M $HClO_4$ with *iR* drop correction.[29] (C) Tafel plots of the kinetic current densities depending on electrode potentials (RHE, reversible hydrogen electrode). (D) The dependence of specific activity, and (E) mass activity (columns, left axis) and specific surface area (filled squares, right axis) on the types of alloys. The electrocatalytic results were obtained by average of three independent measurements with an error margin of <10%.

dx.doi.org/10.1021/cs200328z |*ACS Catal.* 2011, 1, 1355–1359

Pt_3M catalysts have positive shifts of ~40 mV (Figure 4A), which is consistent with the trend of altered electronic structures of these alloys.[5] The observed differences are correlated with the enhanced ORR catalytic activity, and corresponding shifts are also present for the half-wave potentials in polarization curves (Figure 4B). At 0.9 V, the Pt_3M catalysts show improvement factors of ~2−3 in specific activity versus Pt catalyst (Figure 4C and 4D). Among the alloy catalysts, Pt_3Co/C has the highest activity, reaching 3.2 mA/cm^2, versus 3.0 and 2.3 mA/cm^2 for Pt_3Ni and Pt_3Fe, respectively. The volcano-type dependence of catalytic performance on the type of 3d transition metal[5] is revealed in both specific activity and mass activity (Figure 4D and 4E). These findings undoubtedly confirmed the highly homogeneous character of the nanoscale materials synthesized here, which is in line with their solid-solution nature and catalytic behavior of corresponding well-defined extended surfaces.

CONCLUSION

Homogeneous Pt alloy nanocatalysts have been prepared by organic solvothermal synthesis. A uniform distribution of alloy elements, both within individual NPs (forming random Pt_3M solid solution NPs) and on a bulk scale, has been demonstrated by a combination of bulk XRD and HAADF-STEM imaging/EDS elemental mapping. The validation of the catalytic trends that were previously established on extended surfaces has been confirmed for high-surface-area nanocatalysts. The production of highly uniform Pt_3M catalysts is enabled by controlling crucial synthesis parameters such as particle size, alloy composition, and catalyst pretreatment. These findings show that the organic solvothermal method is an advantageous approach toward the synthesis of monodisperse and homogeneous alloy catalysts.

AUTHOR INFORMATION

Corresponding Author

*E-mail: vrstamenkovic@anl.gov.

Funding Sources

This work was conducted at Argonne National Laboratory, a U.S. Department of Energy, Office of Science Laboratory, operated by UChicago Argonne, LLC, under contract no. DE-AC02−06CH11357. This research was sponsored by the U.S. Department of Energy, Office of Energy Efficiency and Renewable Energy, Fuel Cell Technologies Program. Microscopy research was conducted at the Electron Microscopy Center (EMC) for Materials Research at Argonne. HAADF-STEM imaging and EDS analyses were supported by ORNL's SHaRE User Facility, which is sponsored by the Office of Basic Energy Sciences, the U.S. Department of Energy.

REFERENCES

(1) Besenbacher, F.; Chorkendorff, I.; Clausen, B. S.; Hammer, B.; Molenbroek, A. M.; Norskov, J. K.; Stensgaard, I. *Science* **1998**, *279*, 1913–1915.

(2) Diemant, T.; Hager, T.; Hoster, H. E.; Rauscher, H.; Behm, R. J. *Surf. Sci.* **2003**, *541*, 137–146.

(3) Greeley, J.; Mavrikakis, M. *Nat. Mater.* **2004**, *3*, 810–815.

(4) Chen, M. S.; Kumar, D.; Yi, C. W.; Goodman, D. W. *Science* **2005**, *310*, 291–293.

(5) Stamenkovic, V. R.; Mun, B. S.; Arenz, M.; Mayrhofer, K. J. J.; Lucas, C. A.; Wang, G. F.; Ross, P. N.; Markovic, N. M. *Nat. Mater.* **2007**, *6*, 241–247.

(6) Strasser, P.; Koh, S.; Anniyev, T.; Greeley, J.; More, K.; Yu, C. F.; Liu, Z. C.; Kaya, S.; Nordlund, D.; Ogasawara, H.; Toney, M. F.; Nilsson, A. *Nat. Chem.* **2010**, *2*, 454–460.

(7) Tao, F.; Grass, M. E.; Zhang, Y. W.; Butcher, D. R.; Aksoy, F.; Aloni, S.; Altoe, V.; Alayoglu, S.; Renzas, J. R.; Tsung, C. K.; Zhu, Z. W.; Liu, Z.; Salmeron, M.; Somorjai, G. A. *J. Am. Chem. Soc.* **2010**, *132*, 8697–8703.

(8) Maroun, F.; Ozanam, F.; Magnussen, O. M.; Behm, R. J. *Science* **2001**, *293* (5536), 1811–1814.

(9) Burch, R. *Acc. Chem. Res.* **1982**, *15*, 24–31.

(10) Strasser, P.; Fan, Q.; Devenney, M.; Weinberg, W. H.; Liu, P.; Norskov, J. K. *J. Phys. Chem. B* **2003**, *107*, 11013–11021.

(11) Kesavan, L.; Tiruvalam, R.; Ab Rahim, M. H.; bin Saiman, M. I.; Enache, D. I.; Jenkins, R. L.; Dimitratos, N.; Lopez-Sanchez, J. A.; Taylor, S. H.; Knight, D. W.; Kiely, C. J.; Hutchings, G. J. *Science* **2011**, *331*, 195–199.

(12) Stamenkovic, V. R.; Fowler, B.; Mun, B. S.; Wang, G. F.; Ross, P. N.; Lucas, C. A.; Markovic, N. M. *Science* **2007**, *315*, 493–497.

(13) Studt, F.; Abild-Pedersen, F.; Bligaard, T.; Sorensen, R. Z.; Christensen, C. H.; Norskov, J. K. *Science* **2008**, *320*, 1320–1322.

(14) Jankowiak, J. T.; Barteau, M. A. *J. Catal.* **2005**, *236*, 366–378.

(15) Linic, S.; Jankowiak, J.; Barteau, M. A. *J. Catal.* **2004**, *224*, 489–493.

(16) Greeley, J.; Stephens, I. E. L.; Bondarenko, A. S.; Johansson, T. P.; Hansen, H. A.; Jaramillo, T. F.; Rossmeisl, J.; Chorkendorff, I.; Norskov, J. K. *Nat. Chem.* **2009**, *1*, 552–556.

(17) Wang, C.; van der Vliet, D.; More, K. L.; Zaluzec, N. J.; Peng, S.; Sun, S. H.; Daimon, H.; Wang, G. F.; Greeley, J.; Pearson, J.; Paulikas, A. P.; Karapetrov, G.; Strmcnik, D.; Markovic, N. M.; Stamenkovic, V. R. *Nano Lett.* **2011**, *11*, 919–926.

(18) Stamenkovic, V. R.; Mun, B. S.; Mayrhofer, K. J. J.; Ross, P. N.; Markovic, N. M. *J. Am. Chem. Soc.* **2006**, *128*, 8813–8819.

(19) Chen, S.; Gasteiger, H. A.; Hayakawa, K.; Tada, T.; Shao-Horn, Y. *J. Electrochem. Soc.* **2010**, *157*, A82–A97.

(20) Stamenkovic, V.; Mun, B. S.; Mayrhofer, K. J. J.; Ross, P. N.; Markovic, N. M.; Rossmeisl, J.; Greeley, J.; Norskov, J. K. *Angew. Chem., Int. Ed.* **2006**, *45*, 2897–2901.

(21) Schulenburg, H.; Muller, E.; Khelashvili, G.; Roser, T.; Bonnemann, H.; Wokaun, A.; Scherer, G. G. *J. Phys. Chem. C* **2009**, *113*, 4069–4077.

(22) Wang, C.; Wang, G. F.; van der Vliet, D.; Chang, K. C.; Markovic, N. M.; Stamenkovic, V. R. *Phys. Chem. Chem. Phys.* **2010**, *12*, 6933–6939.

(23) Min, M. K.; Cho, J. H.; Cho, K. W.; Kim, H. *Electrochim. Acta* **2000**, *45*, 4211–4217.

(24) Soderberg, J. N.; Sirk, A. H. C.; Campbell, S. A.; Birss, V. I. *J. Electrochem. Soc.* **2005**, *152*, A2017–A2022.

(25) Shevchenko, E. V.; Talapin, D. V.; Rogach, A. L.; Kornowski, A.; Haase, M.; Weller, H. *J. Am. Chem. Soc.* **2002**, *124*, 11480–11485.

(26) Ahrenstorf, K.; Albrecht, O.; Heller, H.; Kornowski, A.; Gorlitz, D.; Weller, H. *Small* **2007**, *3*, 271–274.

(27) Ahrenstorf, K.; Heller, H.; Kornowski, A.; Broekaert, J. A. C.; Weller, H. *Adv. Funct. Mater.* **2008**, *18*, 3850–3856.

(28) Newman, J. S. *J. Electrochem. Soc.* **1966**, *113*, 501.

(29) van der Vliet, D.; Strmcnik, D. S.; Wang, C.; Stamenkovic, V. R.; Markovic, N. M.; Koper, M. T. M. *J. Electroanal. Chem.* **2010**, *647*, 29–34.

(30) Sun, S. H.; Murray, C. B.; Weller, D.; Folks, L.; Moser, A. *Science* **2000**, *287*, 1989–1992.

(31) Sun, Y. G.; Xia, Y. N. *Science* **2002**, *298*, 2176–2179.

(32) Cushing, B. L.; Kolesnichenko, V. L.; O'Connor, C. J. *Chem. Rev.* **2004**, *104*, 3893–3946.

(33) Wang, C.; van der Vliet, D.; Chang, K. C.; You, H. D.; Strmcnik, D.; Schlueter, J. A.; Markovic, N. M.; Stamenkovic, V. R. *J. Phys. Chem. C* **2009**, *113*, 19365–19368.

(34) Chen, J. Y.; Lim, B.; Lee, E. P.; Xia, Y. N. *Nano Today* **2009**, *4*, 81–95.

(35) Wang, C.; Wang, G.; van der Vliet, D.; Li, D.; More, K. L.; Wang, H.-H.; Schlueter, J. A.; Markovic, N. M.; Stamenkovic, V. R. *Adv. Func. Mater.* **2011**, *21*, 147–152.
(36) Mukerjee, S.; Srinivasan, S.; Soriaga, M. P.; Mcbreen, J. *J. Phys. Chem.* **1995**, *99*, 4577–4589.
(37) Ma, Y. G.; Balbuena, P. B. *Surf. Sci.* **2008**, *602*, 107–113.